What the electrocorticogram can tell us about the electroencephalogram

Denise van Barneveld
Supervisors: CCAM Gielen, P Desain, TF Oostendorp

Department of Medical Physics and Biophysics, University of Nijmegen, The Netherlands
Music, Mind and Machine group, NICI, University of Nijmegen, The Netherlands

Although brain signals measured under the skull (electrocorticogram, ECoG) and signals measured on top of the scalp (electroencephalogram, EEG) stem from the same brain activity, they are different. We investigated how we can produce EEG when we know ECoG ("forward problem") and how we can produce ECoG when we know EEG ("inverse problem"). We modeled the head as three concentric spheres, representing the brain, skull and scalp. Brain activity is simulated by a dipole. The forward method links the ECoG potentials on the inner sphere to the EEG potentials on the outer sphere via a transfer matrix, based on the geometries and the conductivities of tissues involved. Results showed that the error between analytically computed EEG and EEG produced from analytically produced ECoG with the forward method, is smaller at electrodes close to the source, compared to electrodes far away from the source. The higher the resolution of an ECoG electrode grid, the better the forward model works. Another finding was that the forward model is more accurate or surface sources, compared to deep sources. This result is of practical importance, since most cognitive interesting sources stem from the cortex (the outermost layer of the brain). In the inverse model, the transfer matrix is inverted and additional regularization constraints are applied to compute ECoG from simulated EEG. We showed that the inverse model gives good results. The forward method is tested with data measured from an epileptic patient at the University of Freiburg. Results show that the forward model gives better results at the EEG electrode overlying the ECoG grid compared to the electrode posterior to the grid. Further research is needed to make errors smaller.

Keywords: *Electroencephalogram, Electrocorticogram, Three-sphere model, Forward problem, Inverse problem, Brain Computer Interface*

Correspondence to: Denise van Barneveld, d.vanbarneveld@student.science.ru.nl

1. Introduction

Many different disorders, such as Amyotrophic Lateral Sclerosis (ALS) and spinal cord injuries, can disrupt the communication between the brain and the peripheral motor system. People most severely affected may lose all voluntary muscle control, including eye movements and respiration. They are totally locked-in to their bodies and are not able to communicate at all. One way to give these patients the possibility to communicate is by a direct brain-computer interface (BCI), which translates brain signals into messages and commands to the external world.

These brain signals can be measured by a variety of methods, e.g. electroencephalography (EEG), invasive electrophysiological methods (like electrocorticogram), magnetoencephalography (MEG), positron emission tomography (PET) and functional magnetic resonance imaging (fMRI). The most common way is to use EEG (e.g. Birbaumer et al., 1999). It has the advantage over the other methods that it is non-invasive, it has a high time-resolution, and it is relatively inexpensive, which makes it is useful for a practical BCI.

1.1 How does a BCI work?

A BCI consists of several parts (Wolpaw et al., 2002). The signal-acquisition part consists of a set (typically between 19 and 128) of recording electrodes that acquire the input (e.g. EEG). These signals are then amplified and digitized. The digitized signals are preprocessed to remove artefacts like line noise and muscle activity.

Then the signals are subjected to one or more feature extraction procedures. A feature is a particular characteristic of the signal, which contains information about the intention or action of the subject. For example, a task could be designed in which imagining movement of the left hand corresponds to "no" and imagining movement of the right hand means "yes". These two conditions correspond to EEG activity in different parts of the brain, which can be considered as different features.

Methods to extract features from EEG are for example spatial filtering, spectral analysis and advanced pattern recognition techniques. BCI can use signal features in the time domain (e.g. evoked potential amplitudes (Farwell & Donchin, 1988)) or in the frequency domain (e.g. mu or beta-rhythm amplitudes (Wolpaw et al., 1991)) or a combination of both. It is also possible to use features like autoregressive parameters that correlate with the user's intention but do not necessarily reflect specific brain events (Wolpaw et al., 2002).

1.2 Classification

The extracted features are usually classified into one of many possible categories. The classified category is translated into device commands that reflect the user's intent. In the example above the features are related to a different topography corresponding to imagining moving the right or the left hand. This is reflected in two classes corresponding to "yes" or "no" or a probability for either class.

Because of the poor signal-to-noise ratio of EEG signals, the classification is usually not perfectly accurate. In a single trial the noise (i.e. the brain signals due to many other processes unrelated to the stimulus) is usually much larger in amplitude than the actual signal (i.e. the brain signals evoked by the stimulus) (figure 1).

Most current BCIs have a computer screen

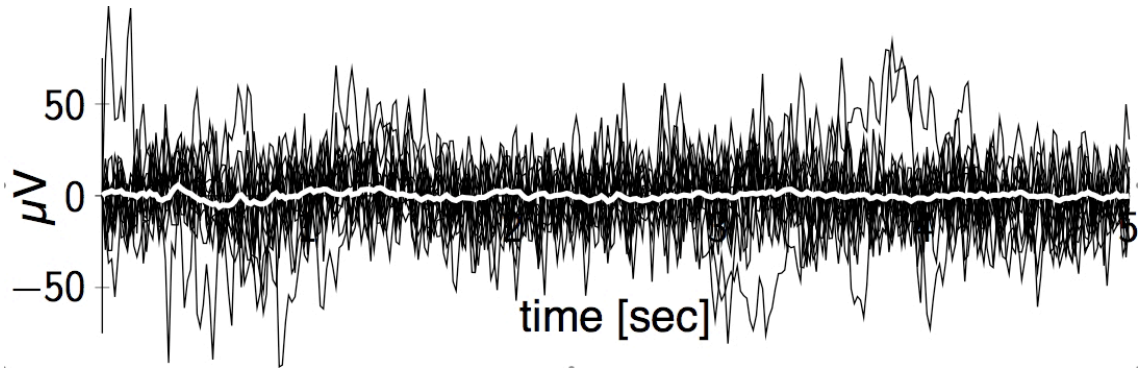

Figure 1 Several single trial EEG signals shown in black, with on top a white signal representing the time locked average of the black trials. This average has a much smaller amplitude than single trials, showing that there is much stimulus unrelated brain activity (noise) in single trials.

as output device, and the output can be the selection of targets, letters or icons presented on it or a cursor moving on the screen. In addition, there are pilot studies exploring BCI control of a neuroprosthesis. For example, Mehring et al. (2003) showed that hand movement target and velocity can be decoded from multiple local field potentials (LFPs), multiunit activity (MUA), or multiple single-unit activity (SUA), for trial-averaged activity as well as single trial data. These signals can be used to reconstruct purposeful arm movements, which can then be used for controlling neuronal motor prostheses. A recently published article by Hochberg et al. (2006) showed another example of the possibility to use neuromotor prosthetics. They describe the implantation of a 10x10 electrode array into the primary motor cortex arm area of a paralyzed man. These electrodes allowed him to move a cursor on a computer screen. With this cursor he could draw, read email, remote control the television, play computer games. Furthermore he could open and close a prosthetic hand. He also performed rudimentary actions with a multi-joint robotic arm.

1.3 Electroencephalogram

As explained above, most BCI applications use EEG-signals. For example, Birbaumer et al. (1999) have developed a communication device that uses slow cortical potentials (SCPs) for electronic spelling. Two locked-in patients with ALS were trained to voluntarily produce changes in their SCPs. The spelling program started with dividing the alphabet in two halves, presented successively on a screen. The subject could select one of the two-letter banks by generating a particular SCP. This bank was split in two and the procedure was continued until only one letter remained selected. When during the procedure a mistake was made, there was the possibility to go back one step by not choosing any bank. Error rates in free spelling were 71.3 and 86.2% in correct selections and 75.0 and 73.7% in correct rejections in two subjects, respectively.

The authors conclude that this study indicates that patients who lack muscular control can learn to control their SCP sufficiently accurately to operate a spelling device with a typing rate of 2 characters per minute.

1.4 Electrocorticogram

Another potential candidate for BCI signal acquisition is electrocorticogram (ECoG). In this technique brain activity is measured directly from the surface of the brain with a grid of electrodes implanted under the skull. Although the signals measured with EEG and ECoG stem from the same activation in the brain, there are several differences between them. Compared to EEG, ECoG:

- has a higher amplitude (50-100 μV versus 10-20 μV)
- has a better signal-to-noise ratio
- has a broader bandwidth (0-200 Hz versus 0-60 Hz)
- has a higher spatial resolution (tenths of millimetres versus centimetres)
- is less vulnerable to artefacts, like muscle artefacts

(Leuthardt et al., 2004). Thus we expect the classification to work better on ECoG signals than on EEG signals. It might also be possible to find different features in the ECoG signals than in EEG.

The major disadvantage of using ECoG for BCI purposes is that ECoG is invasive.

Leuthardt et al. (2004) were the first to demonstrate that ECoG activity recorded from the surface of the brain can enable users to control a one-dimensional computer cursor rapidly and accurately. They used the fact that sensorimotor beta, mu and gamma oscillations change in amplitude in association with actual or imagined movements relative to a condition at rest. ECoG was measured in four epileptic patients when they were either performing or imagining to perform opening or closing the left or right hand, protruding the tongue or saying the word 'move'. Over a brief training period the subjects could use these signals to master closed-loop control. Success rates were between 74 and 100% for actual movements and between 83 and 97% for imagined movements.

In additional open-loop experiments Leuthardt et al. demonstrated that ECoG signals at frequencies up to 180 Hz encoded substantial information about the direction of two-dimensional joystick movements. They conclude that their results suggest that an ECoG-based BCI will be more powerful than an EEG-based BCI and more stable than BCIs that used electrodes implanted in the brain.

1.5 Aim of this study

In the field of electrocardiology much research has been done on the relation between the potentials on the heart surface (epicardium) and those on the body surface.

In previous papers Barr et al. (1977) showed that the potential at the epicardium can be computed from measured potentials on the body surface. The relation between potentials at particular points of the heart surface and potentials at points on the body surface can be related by a linear transformation, the so-called "forward problem". By inverting this relation (the "inverse problem") and applying additional regularization constraints, which is necessary since the relation is mathematically ill posed, the heart potentials can be computed from measured potentials on the body surface with reasonable accuracy (Ramanathan et al., 2004).

We hypothesize that the same method can be used to compute ECoG from measured EEG. This hypothesis will be tested in several steps. First the differences between EEG and ECoG will be calculated with help of the three-sphere model and artificially produced potentials coming from moving dipole sources in the brain (inner sphere). Then the relation between EEG and ECoG will be expressed in terms of transfer coefficients following Barr et al. (1977) to compute EEG from simulated and measured ECoG. Next, this relation will be inverted and additional regularization constraints will be applied to compute ECoG from simulated EEG. The theoretical predictions will be compared to the simulated dipole data, as well as to measurements of ECoG and EEG obtained in an epileptic patient at the University of Freiburg.

2. Methods

2.1 Theory

2.1.1 Source model

A current dipole is an adequate source model for the electric current generated by a small part of the brain. When more parts of the brain are active, the superposition principle holds and each active part may be represented by a separate dipole. Since EEG is most sensitive to radial dipoles, simulations are done for radial dipoles.

2.1.2 Three-sphere model

A common way to model the head is by a three-concentric-sphere model (figure 2). This model represents the brain, skull and scalp as three concentric spheres, with radii of 7.5, 8.0 and 8.5 cm respectively. Each region has its own conductivity with ratios 1, 1/15,1 respectively (Oostendorp et al., 2000). The centre of the spheres is placed in the origin, with the z-axis pointing upwards and the x-y plane is perpendicular to the z-axis.

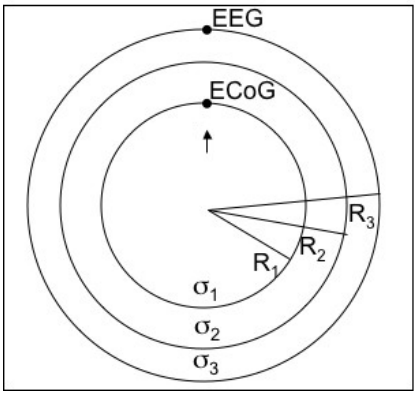

Figure 2 Three-concentric-sphere model. The brain, skull and scalp are represented by three concentric spheres of R1 =7.5 cm, R2 = 8.0 cm and R3 =8.5 cm, with conductivity ratio between the three compartments of $\sigma 1 : \sigma 2 : \sigma 3 =$ 1:1/15:1

Potentials at particular points of the spheres due to a current dipole at a specific place in the inner compartment, the brain, are calculated analytically with the function compute_leadfield in the fieldtrip matlab toolkit[1]. The theory implemented in this function is described in Appendix 2. All potentials will be calculated relative to the potential at a reference point as far from the source as possible, i.e. the point where the sphere crosses the negative z-axis.

2.1.3 Infinite medium

The potential generated by a dipole in an infinite medium, i.e. a theoretical homogeneous medium extending to infinity, is given by:

$$\varphi_\infty(r) = \frac{1}{4\pi\sigma}\frac{\vec{D}\cdot\vec{R}}{R^3} = \frac{1}{4\pi\sigma}\frac{\vec{D}\cos\theta}{R^2} \qquad (1)$$

[1] Fieldtrip toolbox for EEG/MEG-analysis. FC Donders Centre for Cognitive Neuroimaging, Nijmegen, The Netherlands. http://www.ru.nl/fcdonders/fieldtrip

with σ the conductivity of the medium, $\vec{D}$ the dipole moment, $\vec{R}$ the distance from the dipole to the point at which the potential is calculated and θ the angle between $\vec{D}$ and $\vec{R}$ (see figure 3).

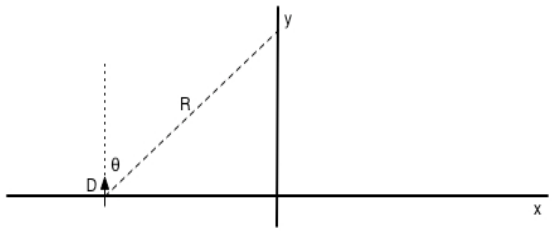

Figure 3 Dipole on x-axis in an infinite medium

Suppose that there is a dipole on the x -axis in an infinite medium (see figure 3), the potential at position $(0,y)$ due to the dipole at $(x,0)$ can be calculated by transforming equation (1) into the following equation:

$$\varphi_{\infty}(y,x) = \frac{D}{4\pi\sigma}\frac{y}{(x^2+y^2)^{3/2}} \qquad (2)$$

where we used that $\cos\theta = y/R$ and $R = \sqrt{x^2+y^2}$

2.1.4 Fourier transformation

The frequency components of a sampled signal $\varphi(t)$ can be computed by taking the discrete Fourier transform of this signal:

$$\varphi(\omega) = \sum_{n=0}^{N-1}\varphi(t)e^{-i2\pi\frac{t}{N}n} \qquad t = 0,\ldots,N-1 \qquad (3)$$

where N is the number of samples. The power spectrum of this signal is:

$$Power(\omega) = \frac{\varphi(\omega)\varphi^*(\omega)}{N} \qquad (4)$$

where $\varphi^*(\omega)$ is the complex conjugate of $\varphi(\omega)$

2.1.5 The forward problem

In this study the forward problem consists of computing the EEG, given a certain ECoG potential distribution. The derivation in Appendix 3 gives the potentials at a certain surface (e.g. EEG), due to potentials at another surface (e.g. ECoG), following Barr *et al.* (1977). This method is called the Boundary Element Method (BEM).

The relation between the potentials on the brain ($\vec{\varphi}$) and the potentials the scalp ($\vec{\psi}$) can be given by (see Appendix 3):

$$\vec{\psi} = \mathbf{T}\vec{\varphi} \qquad (5)$$

The transfer matrix T reflects the transfer coefficients (T_{ij}) between the potential at location *j* on the brain (φ_j) and the potentials at location *i* on the scalp (ψ_i). This matrix is governed by the laws of electrical volume conduction and depends on the volume conductor model, in particular on the geometries and inhomogeneities involved.

2.1.6 Inverse problem

Above we have seen a method to predict EEG from ECoG. The opposite can also be done, which is called the inverse problem. This inverse problem $\vec{\varphi} = \mathbf{T}^{-1}\vec{\psi}$ is an ill-posed problem, since the transfer matrix **T** is close to singular. The most frequently used solution to this problem is to use the Moore-Penrose inverse. This inverse finds the least-squares solution. However, there are more solutions to the problem and the least-squares solution does in general not correspond to the true solution. For example, two small dipoles next to each other will give a different ECoG than one larger dipole in the middle of these two. The EEG is a more attenuated and spatially broader signal than the ECoG. Thus the differences between the EEG signal of two configurations will be small. This makes it difficult to compute the ECoG from the EEG. To solve this ill-posed problem, prior knowledge about the solution has to be used and some anatomical or functional constraints on the infinite solution space have to be imposed. In this study we assume that discontinuities should be avoided. Therefore, we are looking for a smooth solution. By using regularization techniques, the conditioning of the problem can be improved.

2.1.7 Regularization

If a solution should be smooth, the usual regularization implies using the surface Laplacian. This is a restriction of the Laplacian operator to 2-dimensional flat space or to a curved surface in 3 dimensions. In the present study, we take as a regularization operator the surface Laplacian of the function *f*:

$$\Delta_s f = \left(\frac{\partial^2}{\partial x^2} + \frac{\partial^2}{\partial y^2}\right) f \qquad (6)$$

where *x* and *y* are local surface coordinates.

For a triangulated grid, Oostendorp et al have developed a method to approximate the Laplacian (Oostendorp et al., 1989).

2.1.8 Inverse solution

The brain potentials ($\vec{\varphi}$) must obey the relation $\vec{\varphi} = \mathbf{T}^{-1}\vec{\psi}$ and:

$$\Delta_s \vec{\varphi} = \vec{0} \quad (7)$$

The regularized relation between the potentials on top of the scalp ($\vec{\psi}$) and the brain potentials ($\vec{\varphi}$) is then given as:

$$\vec{\varphi} = \begin{bmatrix} \mathbf{T} \\ \lambda\Delta_s \end{bmatrix}^{-1} \begin{bmatrix} \vec{\psi} \\ \vec{0} \end{bmatrix} \quad (8)$$

in which the amount of smoothing can be regulated by the parameter λ.

2.1.9 Triangulations

The Boundary Element Method (BEM) can be applied to volume conductors that are piecewise homogeneous, i.e. consist of a number of compartments with homogenous, isotropic conductivity.

To be able to apply the BEM technique, all boundaries between the compartments involved have to be discretized. Conceptually, it works by constructing a grid over the modelled surface. In this study a triangulated grid is chosen and the potentials are determined only on the vertices of this grid.

First a regularly triangulated sphere with 162 vertices, with the centre being the dipole location, is projected onto the innermost sphere. The BEM assumes the potential differences to change linearly within each triangle. When the potentials change rapidly in space, this assumption is not valid. For this reason, the triangles of this sphere are refined in such a way that the edge of a triangle is divided in two when the variation between $1/r^2$ of the two vertices is more than a certain percentage (worst variation criterion), with *r* the distance between the dipole and the vertex. This inner sphere is inflated to make the other two spheres. Example triangulations are given in figure 4. In this figure the z-axis points to the front upper right.

2.1.10 Interpolation

When the ECoG is only known at some locations on the inner sphere, an interpolation has to be made to estimate the potentials on all points of the inner sphere. The solution of this interpolation is assumed to be a smooth function. One way to construct such a smooth interpolation is to put constraints on the Laplacian of the function.

The estimate of the Laplacian for a triangulated surface can be used (see above), which is expressed in matrix form (Oostendorp et al., 1989):

$$\vec{v} = \mathbf{L}\vec{f} \quad (9)$$

where $\vec{v}$ is a vector containing elements $v_i = (\Delta_s f)_i$, L the Laplacian and $\vec{f}$ the function values, i.e. all potentials on the inner sphere. Not all

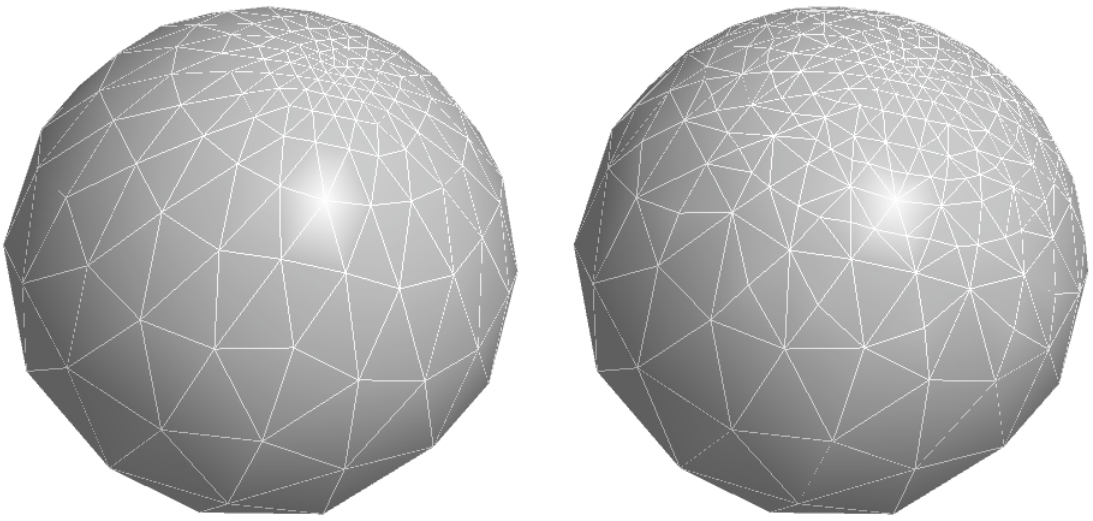

Figure 4 Triangulated spherical surface of dipole position (0,0,0.060) (left) and the same surface refined with a worst variation criterion of 25% (right).

these function values are known. The vector f can be split in two parts, one with the known values, $\vec{f}_1$, $\vec{f}_2$ and with the values that have to be interpolated. In the same way, $\vec{v}$ can be divided in two parts. The Laplacian matrix can be split in four parts:

$$\mathbf{L} = \begin{bmatrix} \mathbf{L_{11}} & \mathbf{L_{12}} \\ \mathbf{L_{21}} & \mathbf{L_{22}} \end{bmatrix} \tag{10}$$

To solve the interpolation, i.e. to find the unknown values $\vec{f}_2$, the following equation has to be solved:

$$\vec{v}_1 = \mathbf{L_{11}}\vec{f}_1 + \mathbf{L_{12}}\vec{f}_2 = \vec{0} \tag{11}$$

This equation is based on the assumption that $\Delta_s \vec{f} = \vec{0}$ at all points were $\vec{f}$ is not given. This method will give an interpolation, which is smooth at unknown points and has sharp peaks at the known points. Minima and maxima are located at points with known potentials (figure 5). In this study this is allowed, under the prior assumption that the extrema of the potentials are located at known points.

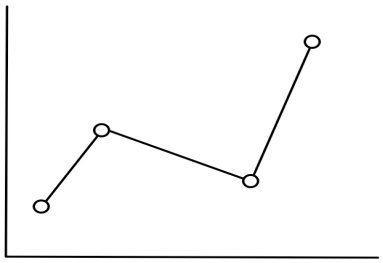

Figure 5 Interpolation. The circles are the known data points and the lines are the interpolation. The interpolations are smooth and there are sharp edges at points were we know the function value, since we assume to be zero only at all points were f is not given.

2.1.11 Quality measure

A measure for the quality of the forward or inverse method is the relative difference between the potentials calculated with the one of these methods and the analytically computed potentials:

$$reldiff = \sqrt{\frac{\sum_i (\varphi_i - \overline{\varphi_i})^2}{\sum_i \varphi_i^2}} \tag{12}$$

where φ_i and $\overline{\varphi}_i$ are, respectively, the analytical and the modelled potentials at point *i* of the brain.

2.2 Experiment – Data collection

2.2.1 Participant

The subject in this study was a patient with intractable epilepsy who underwent temporary placement of subdural electrode arrays to localize the seizure focus prior to surgical resection. She was a right-handed, 19 years old female with no musical background. The subject had no hearing problems. There was no reason to assume cerebral damage.

2.2.2 Electrodes

The patient had a 32-electrode grid (A1 to D8) placed over the left temporal cortex (figure 6) and several electrode strips over the rest of the brain, such that the total number of subdural electrodes was 82. The grid had an inter-electrode distance of 10 mm. The electrodes were made of steel and had a contact diameter was 4.0 mm. Simultaneously EEG was recorded from all 19 standard locations of the standard 10-20 system of electrode placement. Eye movements and muscle activity were also measured.

2.2.3 Data collection/setup

The patient sat in a hospital bed about 75 cm from a laptop screen, and about 75 cm from a loudspeaker (Yamaha MS20). The volume was adjusted to a comfortable level.

The setup consists of a laptop running software called "Presentation"[2] for presenting the stimuli and a standard EEG recording equipment (Neurofile, IT-Med, Usingen, Germany) with a sampling rate of 1024 Hz. These two computers are synchronized via TTL (transistor-transistor logic) pulses triggered at the start and end of the stimuli.

2.2.4 Stimuli

The stimuli were programmed in POCO (D&H) and the resulting MIDI file was converted to audio by Quicktime Musical Instruments using general MIDI commands for low bongo (key 61), velocity 0.7x127 as the metronome and high wood block (key 76), velocity 0.8x127 as the beat.

In the experiment a subject heard an isochronous rhythm of a drum that defined the tempo (figure 7). It continued throughout a trial and functioned as the time-lock metronome. Another

[2] Presentation, http://nbs.neuro-bs.com

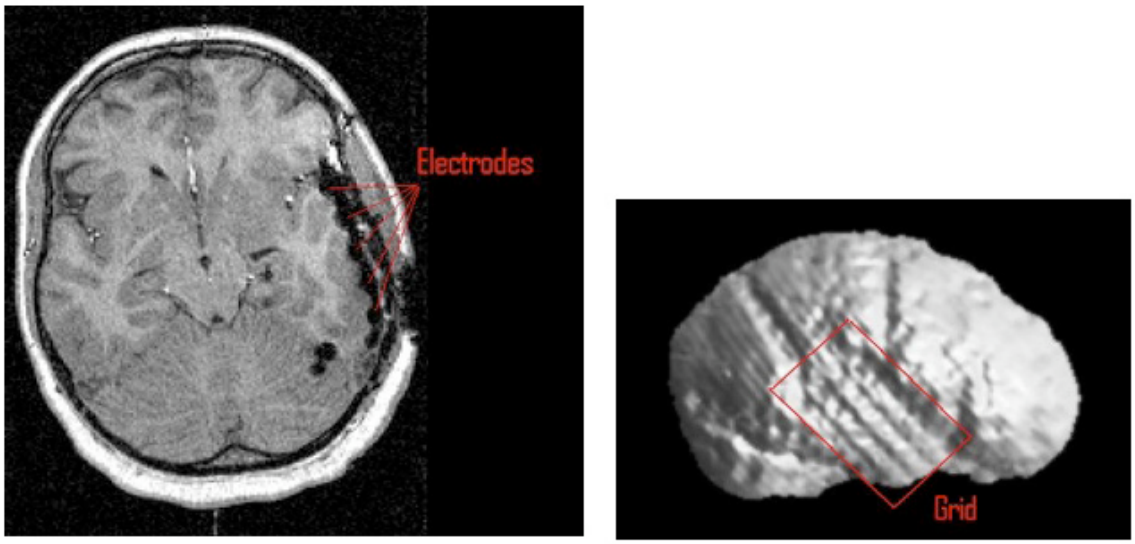

Figure 6 Electrode locations seen in a axial MRI slice (left) and on the outer surface of the brain (right) of the subject.

higher drum was heard once every two, three or four beats and gave an accent to the beats. After three repeats there was one accent played softer and eventually there were no accents played anymore. The subject had to imagine that the accent was still there. At the end of the sequence an accent tone (probe) sounded. The subjects had to indicate whether this probe was on an imagined accent or not. This task was to control attention and to check whether the subject was still on-track.

Per block, the stimuli were randomly played one after each other. The next rhythm started when the subject hit a button (self-paced). We recorded three blocks of 36 stimuli, all with the same order of stimuli.

Before the real experiment started, there was a practice part. In this part the rhythms were easier. There were more accents played before the higher drum fades, this fading lasted longer and the imagery part was shorter. It was important to make sure that the subject understood the task. To account for this, the end of the practice block was determined as follows. We set a counter, which counted the correct answers. Whenever the subject made a mistake, the counter was set two back. The practice block ended when the counter had a value of five.

2.2.5 Event related potential

In a single trial, data contains much brain activity unrelated to the stimulus, which we will call noise. To reduce this noise, an event related potential (ERP) is produced. This ERP is constructed from perception data from an accented tone of a two beat rhythm. We used data from 100 ms before this tone until 500 ms after this tone, which we will call trials for brevity. First all trials with artefacts (like eye movements) are removed. In the resulting 87 trials we removed the line noise of 50 Hz. Then we performed baseline correction to remove differences in impedance of electrodes, by subtracting the mean of the 100 ms period before the stimulus. Last the trials are averaged to produce

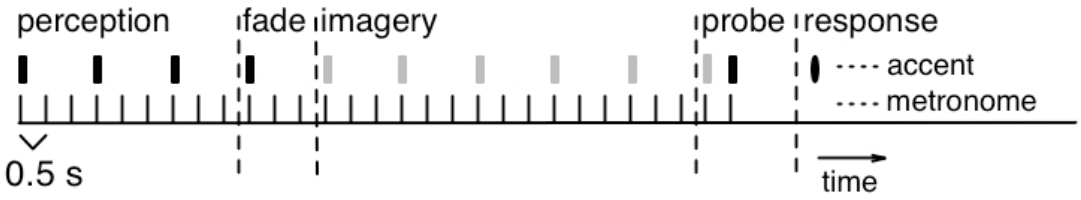

Figure 7 An example stimulus. The horizontal line is the time axis. The lower row shows the metronome ticks. Thick black blocks represent accented tones and grey blocks the imagined accents. The black oval represents the response that has to be given.

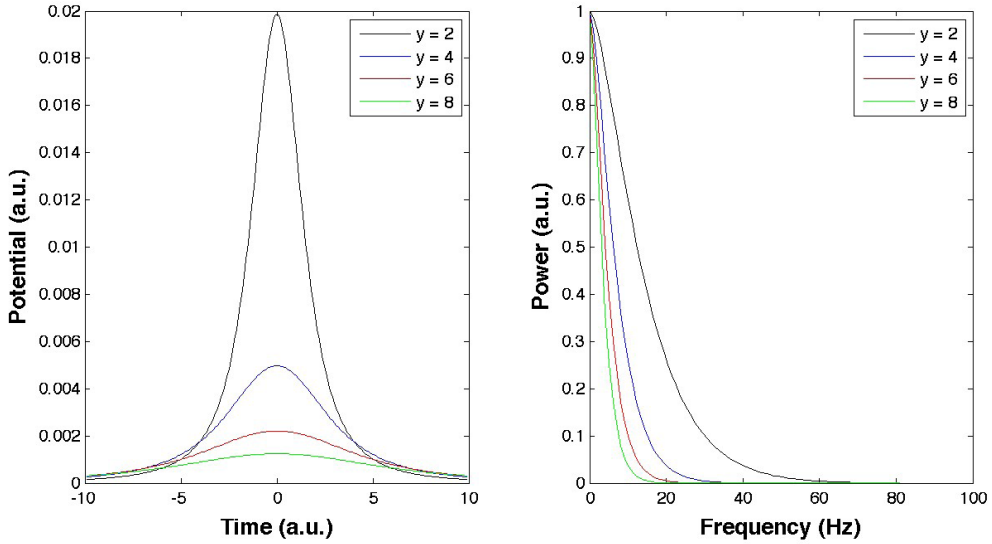

Figure 8 The left panel shows the potentials at different normalized distances y, due to a normalized dipole running with v =1 s-1 along the x-axis of an infinite medium of conductivity 1S. The right figure gives the normalized power in the frequency domain of the potentials from the left figure.

an ERP. Averaging cancels out brain activity unrelated to the stimulus.

All event related potentials are referenced to electrode O1. This electrode is situated at the backside of the head, far away from the grid and the auditory cortex.

3. Results

3.1 Potentials in infinite medium

Figure 8 shows the simulated potentials due to a dipole with a normalized dipole moment moving along the x-axis of an infinite medium with a conductivity of 1 S for different positions on the y-axis. The larger the distance from the dipole, the smaller the amplitude of the signal and the broader the peak of the signal. This results in a higher frequency content in signals at points closer to the source.

3.2 Differences between EEG and ECoG

The simulated ECoG and EEG potentials measured on (0,0,0.075) and (0,0,0.085),

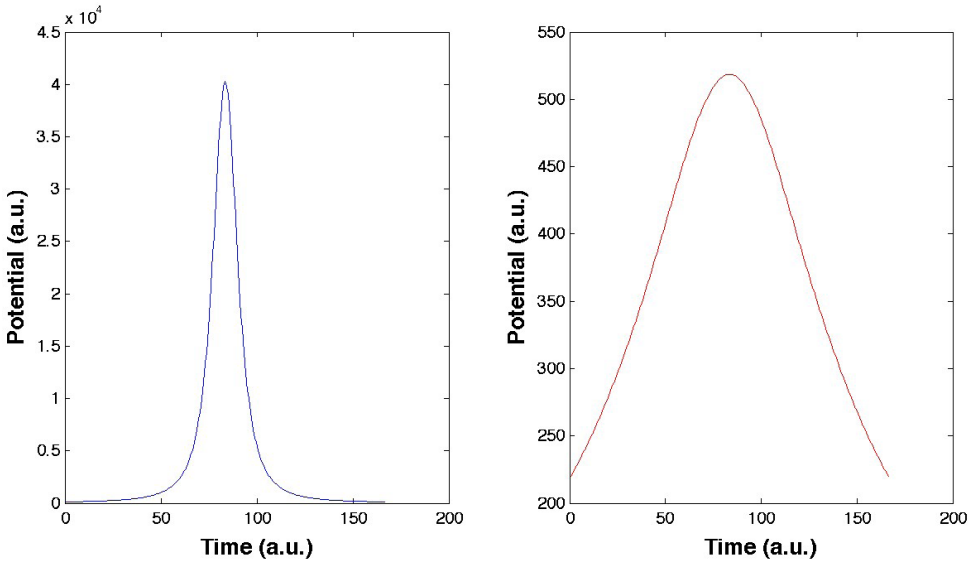

Figure 9 Simulated ECoG (left) and EEG signal (right) from running dipole with m and s-1 in the inner sphere of the three-concentric sphere head model.

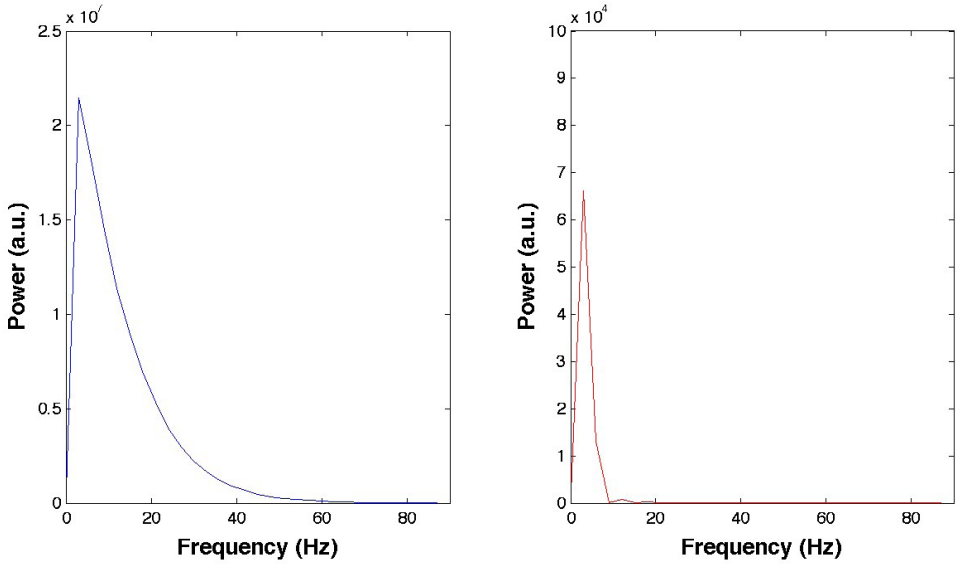

Figure 10 Power spectra of the signals in figure 9.

respectively, due to the moving dipole $\vec{D}(\vec{x},t) = D_0(\vec{x}_0 - \vec{v}t)$ with $\vec{x}_0$ =(0, -0.017, 0.073) and $\vec{v} = (0,2.0 \cdot 10^{-4},0)$ s^{-1} are given in figure 9.

There are two important differences between these signals. The EEG signal is broader in time and about 80 times smaller in amplitude than the ECoG signal. This has two reasons. The distance to the dipole is larger at the EEG electrode compared to the ECoG electrode. The second reason, that has the largest influence here, is the large resistance of the skull that causes the potentials to attenuate and to smear.

3.3 Influence of the skull on EEG

Figure 11 shows the smearing properties of the The broader the signal, the less high frequencies are present in the frequency spectrum of the signal. This is made visible in the power spectra of the two signals (see figure 10).

skull due to its low conductance. In the left figure the skull conductance was taken the same as the conductance of the brain and scalp. This resulted in a smaller region with high potentials than when the skull conductance was taken 1/15 of the brain and scalp conductance (right figure). This

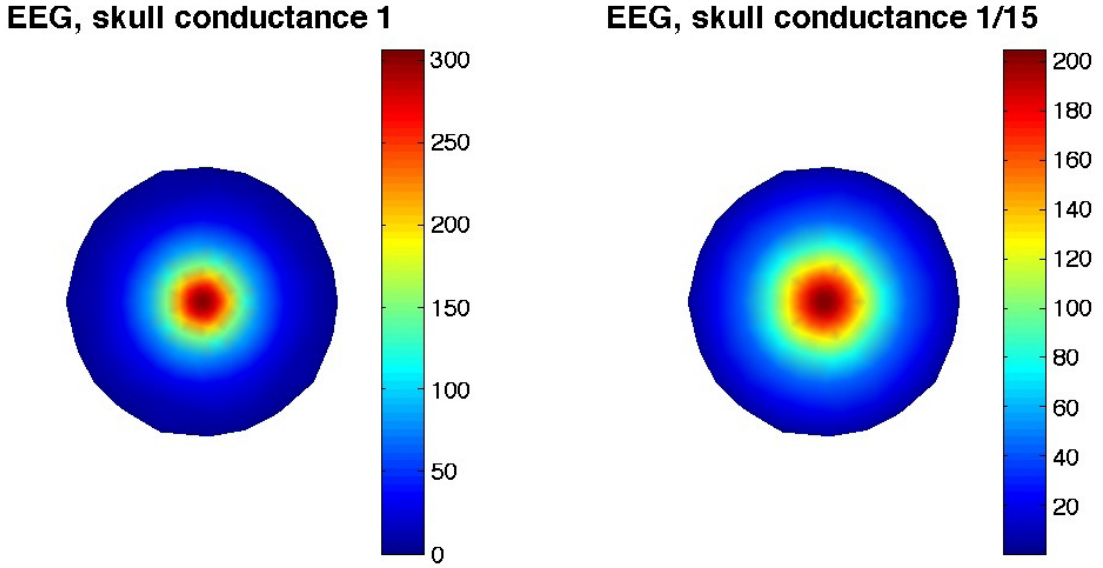

Figure 11 The influence of the skull conductance on the topography of the EEG. The left figure shows EEG potentials for a dipole at (0,0,0.060) in a.u. with a skull conductance of 1S, the same as the brain and the scalp. The right figure shows the same for a skull conductance of 1/15S, the actual conductivity of the skull (Oostendorp et al., 2000)

figure also shows the attenuation of the signal due to the lower conductivity, in the right figure versus the left one (notice the scale differences).

3.4 Forward problem – Predicted EEG from simulated ECoG

In the next section, EEG on all vertices of the triangulated outer sphere is calculated from simulated ECoG with the forward method. Simulation data is obtained for four dipole locations: (0,0,0), (0,0,0.020), (0,0,0.040), (0,0,0.060). All dipoles are of unit strength and pointing in the z-direction.

For the four dipole locations, the following worst variation criteria were used 4%, 12%, 20% and 25%, which resulted in spheres with 162, 366, 442 and 839 vertices, respectively.

For brevity we define the analytically produced potentials according to equation (20) as "true EEG potentials" and we will refer to the potentials calculated with the forward method according to equation (5) as "predicted EEG potentials". Figures 12 to 15 show true values (upper left), the predicted EEG potentials (upper right), the differences between the predicted and the true values (lower left) and these differences relative to the true potentials (lower right) colour coded on the outer sphere, for the four dipoles respectively. Red colours mean high values and blue colours mean low values, as given in the colour bar at the right side of the spheres values. The z-axis is pointing towards the reader. The potentials are referenced to the electrode on the negative z-axis.

The topography of the true values and the predicted potentials are very similar. They both start at zero at the negative z-axis (this part is not visible in the figures) and increase to positive at the positive z-axis. For all dipoles the predicted values are slightly larger than the true values. This results in relative differences between the analytically computed values and the values produced with the forward method of 7.5, 6.6, 7.9 and 11% for dipoles at (0,0,0), (0,0,0.020), (0,0,0.040) and (0,0,0.060) respectively.

The forward method is not completely accurate. This has two reasons. First there is an error in the analytically calculated ECoG. By computing the ECoG, we represented the brain as a sphere in a

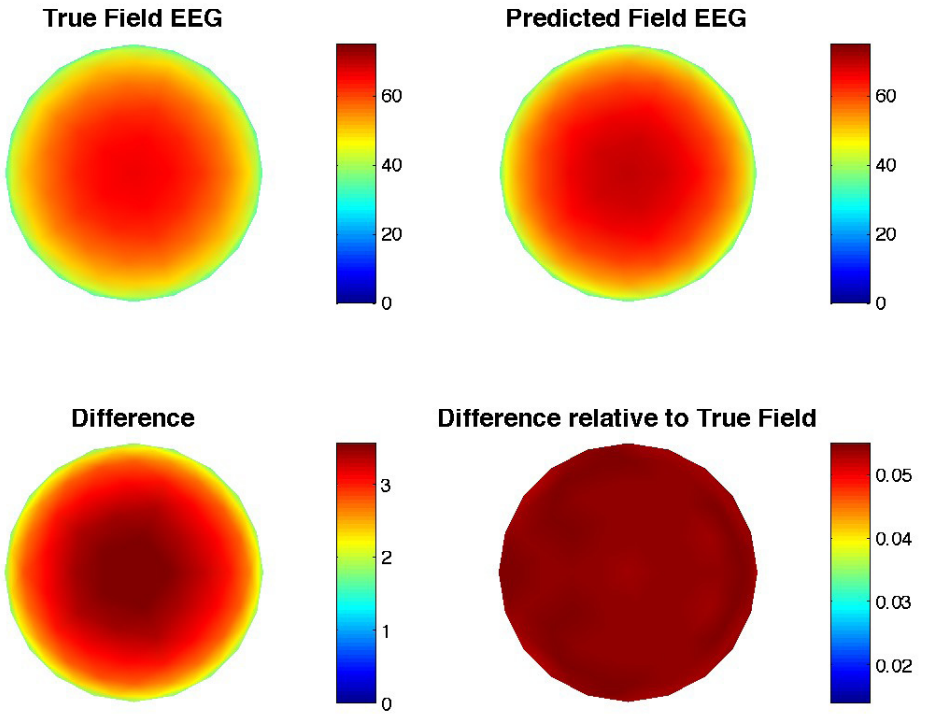

Figure 12 Predicted EEG from simulated ECoG data (upper right, in a.u.) compared to true EEG (upper left, in a.u.) from dipole at (0,0,0), relative difference is 7.5%. The differences between the predicted and the true values (in a.u.) and these differences relative to the true EEG are given in the lower left and right figure, respectively.

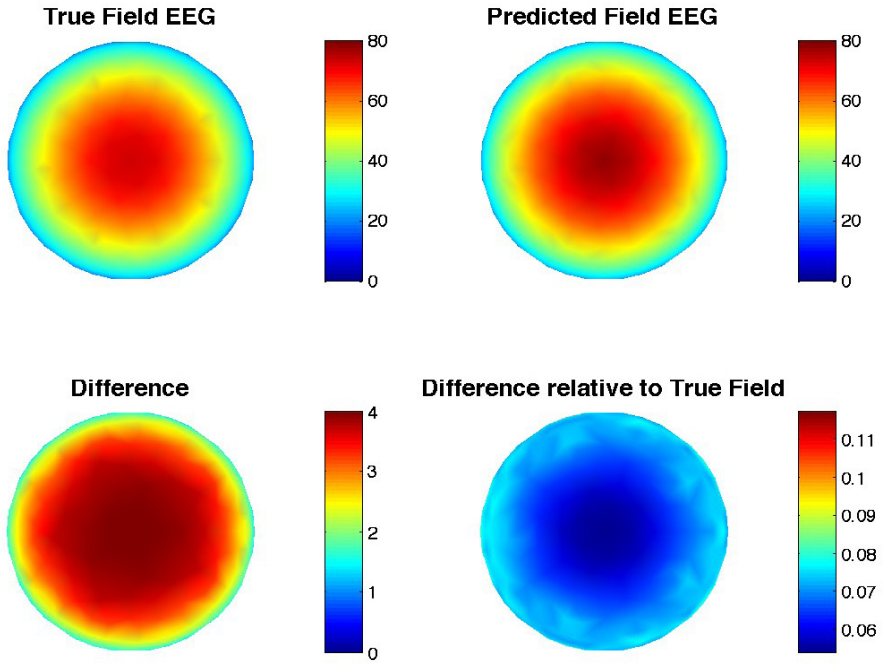

Figure 13 Predicted EEG from simulated ECoG data (upper right, in a.u.) compared to true EEG (upper left, in a.u.) from dipole at (0,0,0.020), relative difference is 6.6%. The differences between the predicted and the true values (in a.u.) and these differences relative to the true EEG are given in the lower left and right figure, respectively.

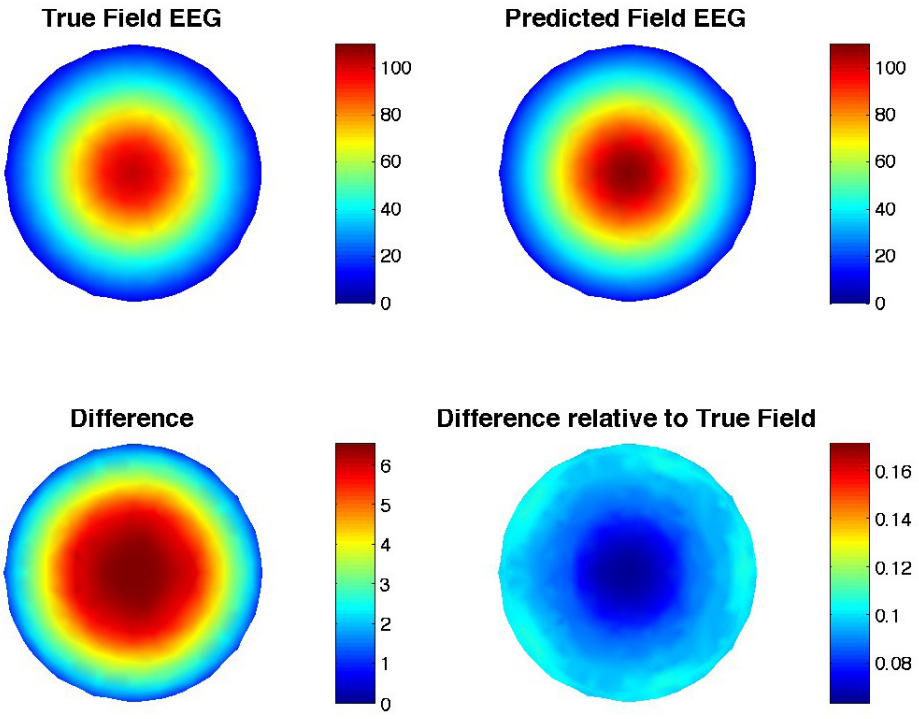

Figure 14 Predicted EEG from simulated ECoG data (upper right, in a.u.) compared to true EEG (upper left, in a.u.) from dipole at (0,0,0.040), relative difference is 7.9%. The differences between the predicted and the true values (in a.u.) and these differences relative to the true EEG are given in the lower left and right figure, respectively.

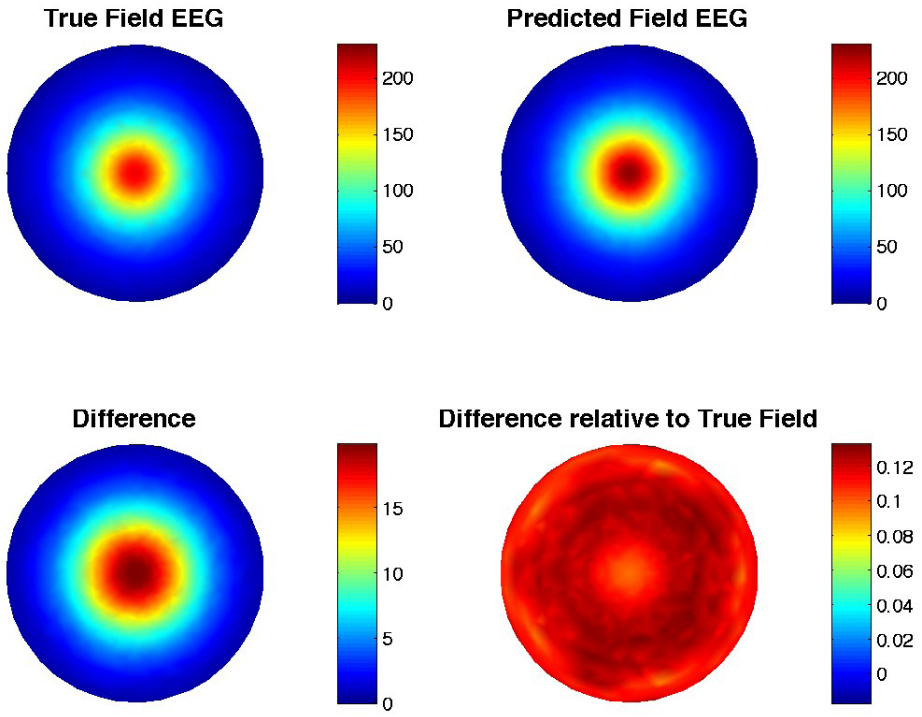

Figure 15 Predicted EEG from simulated ECoG data (upper right, in a.u.) compared to true EEG (upper left, in a.u.) from dipole at (0,0,0.060), relative difference is 11%. The differences between the predicted and the true values (in a.u.) and these differences relative to the true EEG are given in the lower left and right figure, respectively.

non-conducting medium ignoring the skull and the scalp. This results in an overestimation of the ECoG potentials, which results in the end in an overestimation of the predicted EEG potentials Another reason for the relative difference is the numerical implementation. The surface is discretized, which causes small discrepancies in the potentials. These discrepancies are larger with more complex and non-symmetrical geometries. Dipoles further from the origin of the spheres have more complex triangulated spheres, which results in larger errors in the predicted EEG potentials.

The lower left panels of figures 12 to 15 show that the absolute differences are larger at points overlying the source, than at points far away from the source. The explanation is that the true potentials as well as the predicted potentials are referenced to the electrode furthest from the source. This makes the potentials at this point the same at the two surfaces by design.

Another way to look at the differences is the difference relative to the true values (lower right panels of figures 12 to 15). These are larger at points further from the source than at points overlying the source. This means that the predictions are better at points overlying the source, which are the most interesting points to predict for BCI purposes.

Another observation is that more eccentric dipoles have smaller areas with large potentials.

3.5 Forward problem – Predicted EEG on grid from ECoG on grid

In the previous section, ECoG potentials were simulated at all vertices of the inner sphere. In reality ECoG cannot be measured all over the brain. It will be measured with a grid of electrodes over a small part of the cortex. This setup is simulated in this section. We analytically calculate ECoG potentials only on a square grid placed on the triangulated inner sphere. This is used in the forward model to produce EEG on a similar grid on the outer sphere, via a transfer matrix. We investigate how the relative difference between analytically produced EEG potentials and the predicted EEG potentials depends on the size of the EEG and ECoG grids, the ECoG electrode

distance and the dipole position.

3.5.1 ECoG grid construction

A square ECoG grid is placed on the inner sphere with the middle electrode placed on the positive z-axis. We constructed ECoG grids of different sizes: a small sized grid of 0.030 x 0.030 m, a medium sized grid of 0.050 x 0.050 m and a large sized grid of 0.060 x 0.060 m. Within each of these grids we varied the electrode distance. The grids with the largest electrode distance (0.030, 0.050, 0.060, for the small, medium and large sized grids, respectively) consist of five electrodes, placed on the four edges of the grid and one electrode in the centre. A more refined grid consists of 3x3 electrodes on these same small, medium and large sized grids, with an inter electrode distance of 0.015, 0.025 and 0.030 respectively. Grids with smaller electrode distances consist of 5x5, 7x7 and 9x9 electrodes placed on these small, medium and large sized grids, with electrode distances as given in Table 1.

Table 1 ECoG grid sizes

Amount of Electrodes	Small Electrode distance (m)	Medium Electrode distance (m)	Large Electrode distance (m)
2x2 plus middle	0.030	0.050	0.060
3x3	0.015	0.025	0.030
5x5	0.0075	0.013	0.015
9x9	0.0038	0.0063	0.0075
17x17	0.0019	0.0031	0.0038

3.5.2 EEG grid construction

The EEG grid size is varied too. First one electrode is placed at the outer sphere right above the centre of the ECoG grid, thus on the positive z-axis. A larger EEG grid consists of a row of electrodes placed around the EEG electrode, resulting in a 3x3 grid of 0.020 x 0.020 m. The middle electrode of this grid is still located right above the middle of the ECoG grid. Then this grid is expanded by one row of electrodes placed around the 3x3 grid, resulting in a 5x5 grid of 0.040 x 0.040 m. This procedure is repeated to create a 7x7 grid of 0.060 x 0.060 m and finally a 9x9 grid of 0.080 x 0.080 m.

3.5.3 Interpolation

The ECoG is produced analytically only at the electrodes of the square ECoG grid. The forward model needs potentials at all vertices of the whole inner sphere. The unknown potentials have to be estimated by interpolation (see Method section). In these interpolations we assume the potential at the electrode on the negative z-axis to be zero.

Figure 16 gives an example of interpolation for a medium sized ECoG grid and a dipole at (0,0,0). The left panel shows the analytically produced ECoG values, which we will refer to as "true values ECoG", projected on a sphere, with the z-axis pointing towards the reader. The middle panel shows the interpolated ECoG potentials for an ECoG grid of only five electrodes with an electrode distance of 5.0 cm. The right panel shows the interpolated values estimated from an ECoG grid of 17x17 electrodes with an electrode distance of 0.31 cm. The higher the ECoG grid resolution, the better the interpolation: the topography of the right figures look much more like the true values than the topography of the middle figure.

Figure 17 show the same for a small sized ECoG grid and a dipole placed at (0,0,0.060). The potentials are estimated more accurately with a higher resolution ECoG grid, because the Laplacian cannot describe the rapid potential changes on the grid. The middle and right panel show that the decay in potential to zero from the edge of the grid to the backside of the sphere is not fast enough. This is due to the applied Laplacian, which assumes a smooth interpolation between successive points and maxima at points with known potential.

Figure 18 shows the relative differences between the interpolated potentials and the ECoG potentials analytically calculated on all vertices as function of ECoG electrode distance, for different ECoG grid sizes and different dipoles. In general, interpolations are better for dipoles closer to the origin. The

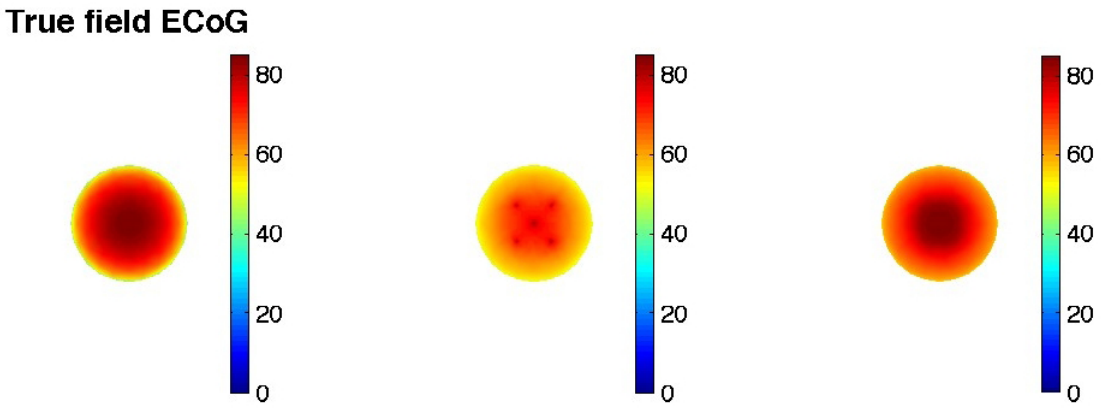

Figure 16 An example of two interpolations. Medium grid, ECoG electrode distance of 5.0 cm (middle, in a.u.) and 0.31 cm (right, in a.u.) for a dipole at (0,0,0) compared to true values (left, in a.u.).

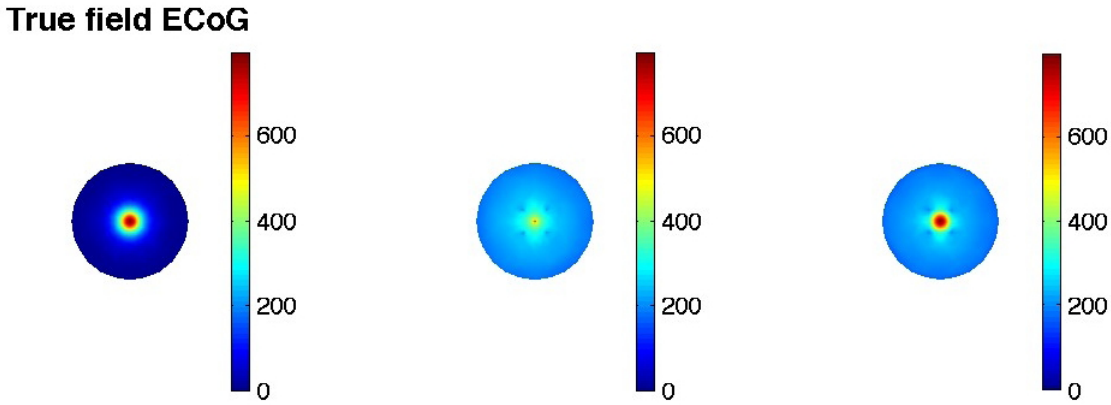

Figure 17 An example of two interpolations. Small grid, ECoG electrode distance of 3.0 cm (middle, in a.u.) and 0.19 cm (right, in a.u.) for a dipole at (0,0,0.060) compared to true values (left, in a.u.).

closer the dipole to the origin, the smoother the potential surface, and the better it can be described by the Laplacian (compare figure 16 and 17). The electrode distance has a large influence if the potential changes rapidly over the grid, like for a dipole at (0,0,0.060). These rapid changes cannot be described by the Laplacian and thus cannot be interpolated well (compare the middle and left panel of figure 17).

The grid size has not much influence on the relative difference, except for the dipole at (0,0,0.060). Here the interpolation with a large grid is more accurate than with smaller grids. The reason for this is that the potentials at the edge of the large grid are closer to zero than at a smaller grid. This results in a smaller overestimation of the potentials from the edge of the grid to the backside of the sphere for large grids compared to small grids.

3.5.4 Results EEG

The interpolated potentials are used in the forward method to predict the corresponding EEG potentials. For brevity we will refer to the analytically produced EEG with equation (20) as "true EEG potentials" and to the EEG potentials computed with the forward method (equation (5)) as "predicted EEG potentials".

Figure 19 shows the relative difference between the true values and the predicted EEG potentials for different dipole positions as a function of the ECoG electrode distance and EEG grid size. In general, the further the source is from the surface, the larger the relative difference. For deeper sources, the interpolated potentials at points at the backside of the ECoG sphere, around the negative z-axis, are too high. This causes the EEG potentials at points at the backside of the EEG sphere to be overestimated. Afterwards, potentials are referenced to the EEG electrode on the negative z-axis, which causes the potentials on the grid to drop more than needed. This effect is less for surface dipoles, since the interpolated ECoG potentials at the backside of the sphere are close to zero.

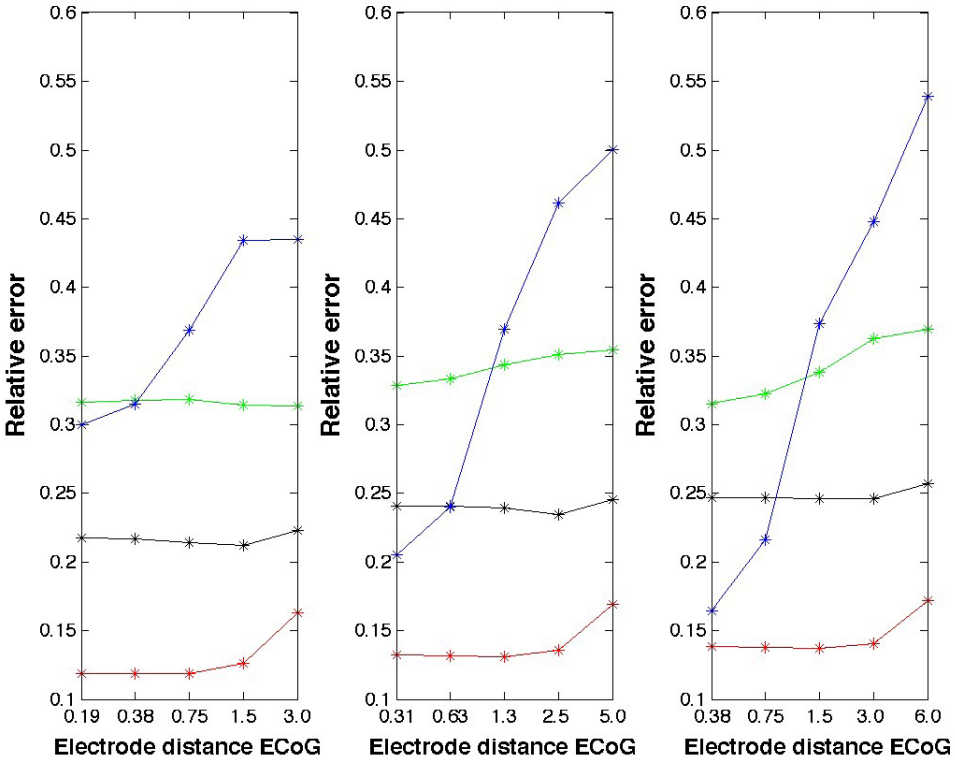

Figure 18 Relative difference between the true values of ECoG and the interpolated ECoG, for different ECoG electrode distances (in cm), for four different dipoles: (0,0,0) in red, (0,0,0.020) in black, (0,0,0.040) in green and (0,0,0.060) in blue and three different grid sizes: small (left), medium (middle) and large (right).

This is illustrated in figure 20 and 21. These figures show the true EEG potentials (left panel) and the predicted EEG potentials (right panel) from simulated ECoG data on a medium size grid from a dipole at (0,0,0.040) and a small sized grid with dipole position (0,0,0.060) respectively. The x,y-plane represents the 9x9 EEG grid and the z-axis the potentials on the points of the grid. In the right panel of figure 20, the middle EEG electrode has a lower potential than the analytically computed potential on that electrode (left panel). Whereas in figure 21, the predicted potential at the middle electrode has only a small difference compared to the analytical value. This shows that the surface dipole is less influenced by overestimation of the reference electrode.

Another observation in figure 19 is that the relative error decreases only slightly with increasing ECoG electrode resolution. Especially for a dipole at (0,0,0.060) this parameter has a large influence on interpolation, whereas its influence on EEG prediction is small. The reason can be that due to the smearing of the skull, the differences in predicted EEG due to these different ECoG configurations are small.

For the small ECoG grid with electrode distance 0.0019m and dipole (0,0,0.060), we see an enormous increase in relative difference with increasing EEG range (figure 19). The corresponding EEG potentials of this example are given in figure 21. In the middle of the grid (which corresponds to an EEG grid with one electrode) the predictions are accurate, whereas on the edge the predicted potentials are far too high (which corresponds to an EEG grid with 9x9 electrodes) compared to the true EEG potentials. This is due to the overestimated ECoG potentials from the edge of the grid to the backside of the sphere (figure 17, right).

3.6 Inverse problem – Predicted ECoG from simulated EEG

In this section ECoG on all vertices of the innermost sphere is calculated from the EEG on the outer sphere via a transfer matrix with additional regularization constraints. The four same dipoles as before are used, with worst variation

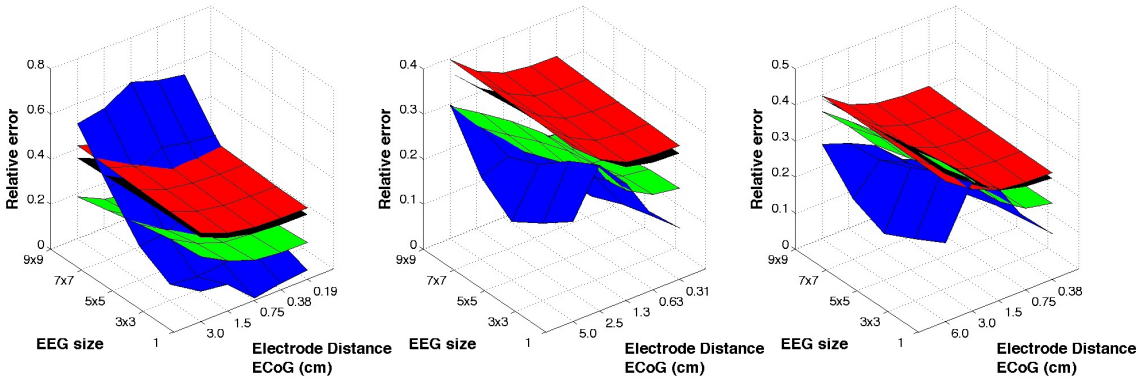

Figure 19 Relative difference between true values EEG on the grid and predicted values from simulated ECoG data on different grids: small (left), medium (middle) and large (right), for different dipoles (0,0,0) in red, (0,0,0.020) in black, (0,0,0.040) in green and (0,0,0.060) in blue as function of the ECoG electrode distance (in cm) and EEG grid size.

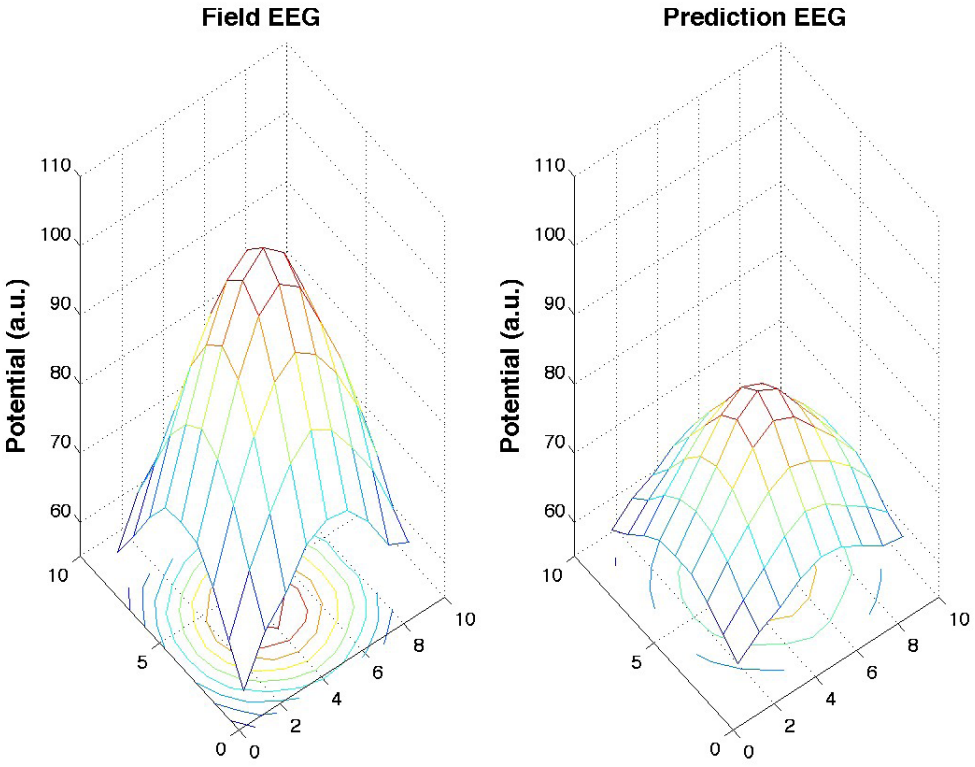

Figure 20 An example of true EEG potentials compared to potentials predicted from simulated ECoG data on a medium grid for a dipole at (0,0,0.040). The x,y-plane is the grid, with the potentials on places on this grid set on the z-axis.

criteria of 4%, 20%, 30% and 35%. This resulted in spheres with 162, 162, 177 and 465 vertices, respectively.

Good smoothing parameters (λ, equation (8)) have to be found. Large parameters will give smoother potential surfaces than small parameters, but a smooth potential surface is not always the best. In this part best results were obtained with regularization parameters of 10^{-6}, 10^{-6}, 10^{-7} and 10^{-5} for dipoles at (0,0,0), (0,0,0.020), (0,0,0.040) and (0,0,0.060) respectively.

Like in the forward method section, we will refer to the analytically produced potentials by equation (20) as "true ECoG potentials" and to the potentials produced with the inverse method according to equation (8) as "predicted ECoG potentials".

Figures 22 to 25 show the true ECoG potentials

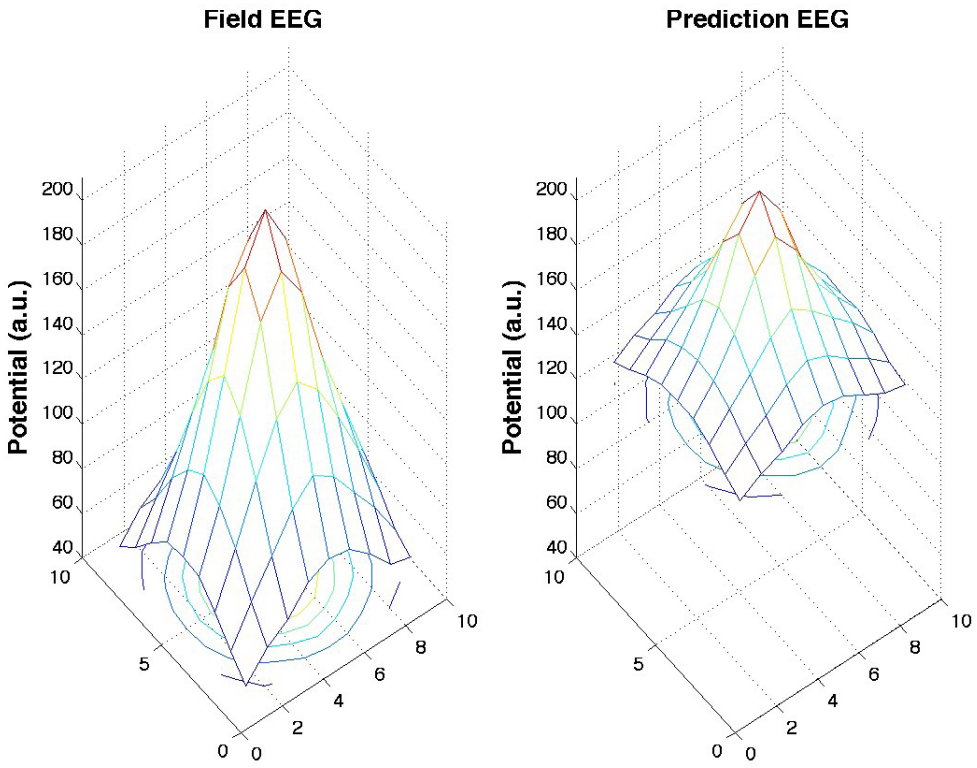

Figure 21 An example of true EEG potentials compared to potentials predicted from simulated ECoG data on a small grid for a dipole at (0,0,0.060). The x,y-plane is the grid, with the potentials on places on this grid set on the z-axis.

(upper left), the predicted ECoG potentials (upper middle) and the differences between the predicted and the true values (true-prediction) (upper right) colour coded on the inner sphere, for the four different dipoles successively. The z-axis is pointing towards the reader. Red colours mean high potentials and blue colours mean low potentials, corresponding to the colour bar at the right side of the spheres (note the scale differences between the different plots). Potentials are referenced to the electrode on the negative z-axis.

Like with the forward method the topographies of the true values and the predicted potentials look rather similar. They both start at zero at the negative z-axis (the part that is not visible in the figures) and increase to positive at the positive z-axis. Different from the forward method, in the inverse method the predicted values are in general slightly lower than the true values (note the scale differences between (upper left) and (upper middle)). This results in relative differences between the analytically computed values and the values produced with the inverse method of 4.1, 5.8, 7.5 and 7.7% for dipoles at (0,0,0), (0,0,0.020), (0,0,0.040) and (0,0,0.060) respectively. The differences between the predicted and true values ECoG (upper right) are small compared to the potentials. The absolute differences are higher at points overlying the source compared to points far away from the source, but the difference relative to the true potentials has no general topography like we have seen in the forward method. The reasons for these relative differences are the same as we have seen in the forward method: the numerical implementations and the error in the analytically produced ECoG.

The predicted ECoG values are used in the forward method to give a control EEG. If no, too low or too high regularization parameters are used, the relative difference between the true EEG and control EEG will be large, whereas in the ideal case both are exactly the same. The lower panels of figures 22 to 25 show the potential distributions over the spheres of true EEG (left) and control EEG (middle). Relative differences between the control EEG and true EEG are below 10^{-5} % for dipoles at (0,0,0), (0,0,0.020), (0,0,0.040). These differences are due to numerical implementations. The relative difference between the control EEG and true EEG for the dipole at (0,0,0.060) is 0.01%.

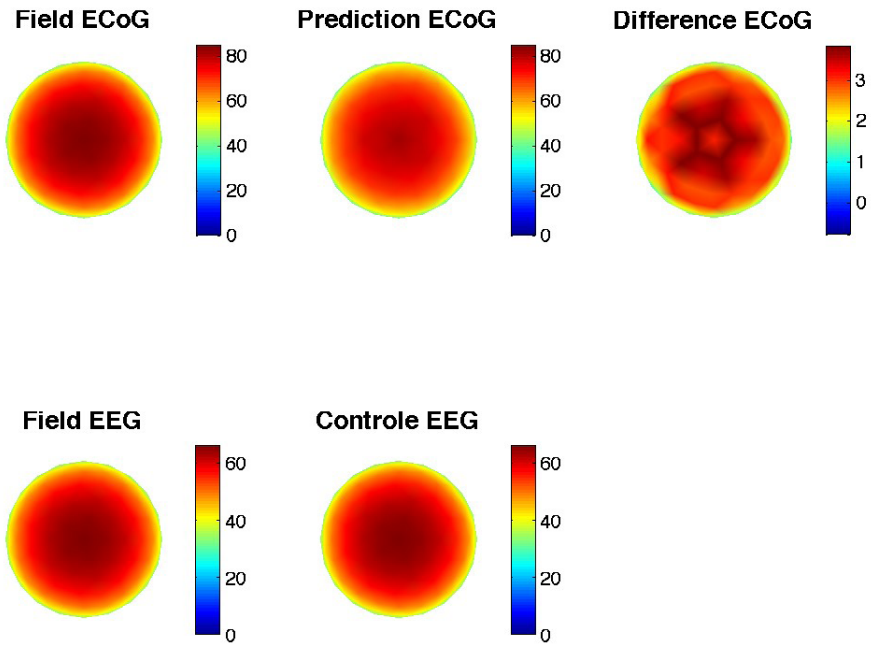

Figure 22 Predicted ECoG from simulated EEG data (upper middle, in a.u.) compared to true ECoG from dipole at (0,0,0) (upper left, in a.u.) and the difference between these two potentials (upper right, in a.u.). Predicted control EEG from predicted ECoG (lower middle, in a.u.) compared to true EEG (lower left, in a.u.).

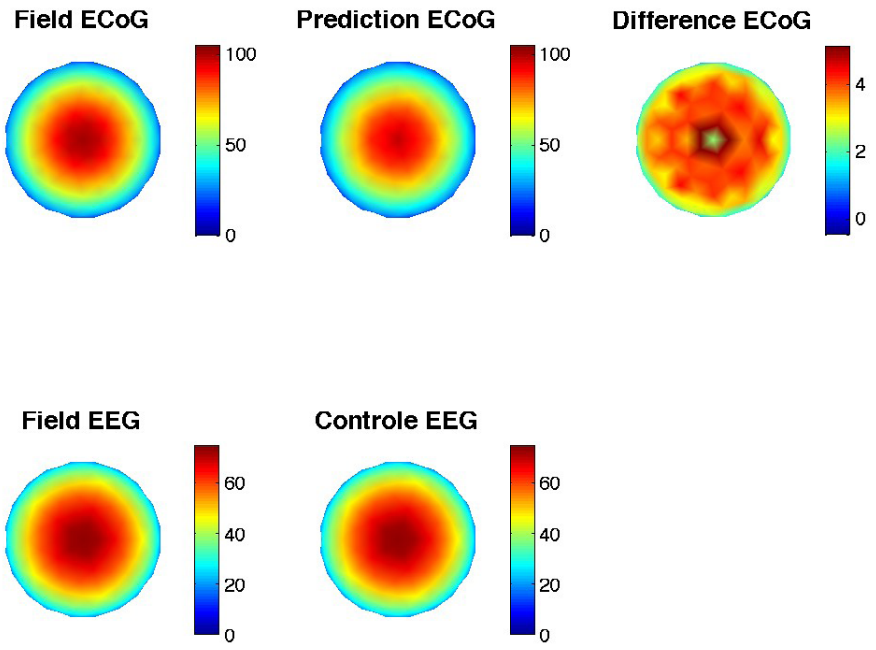

Figure 23 Predicted ECoG from simulated EEG data (upper middle, in a.u.) compared to true ECoG from dipole at (0,0,0.020) (upper left, in a.u.) and the difference between these two potentials (upper right, in a.u.). Predicted control EEG from predicted ECoG (lower middle, in a.u.) compared to true EEG (lower left, in a.u.).

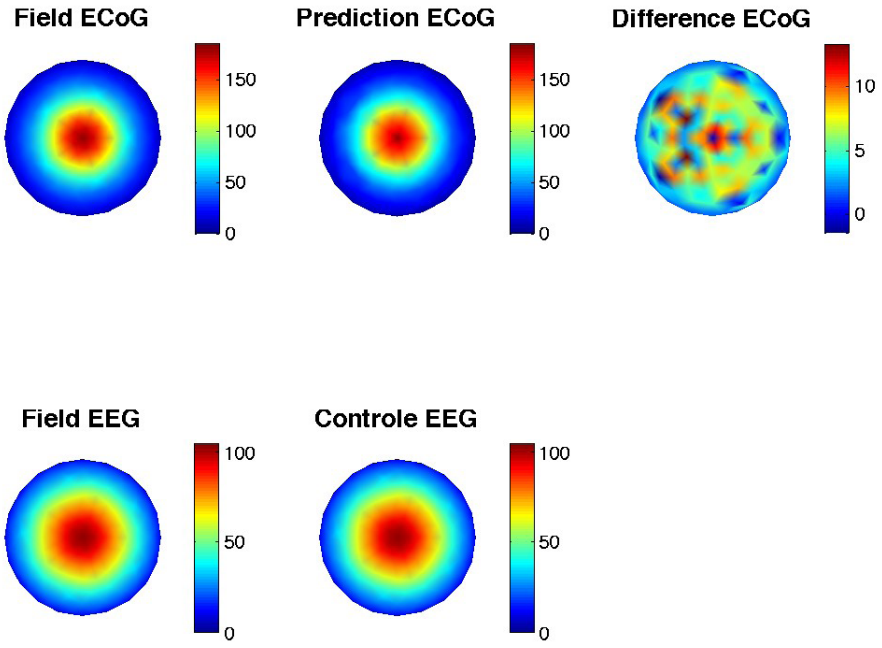

Figure 24 Predicted ECoG from simulated EEG data (upper middle, in a.u.) compared to true ECoG from dipole at (0,0,0.040) (upper left, in a.u.) and the difference between these two potentials (upper right, in a.u.). Predicted control EEG from predicted ECoG (lower middle, in a.u.) compared to true EEG (lower left, in a.u).

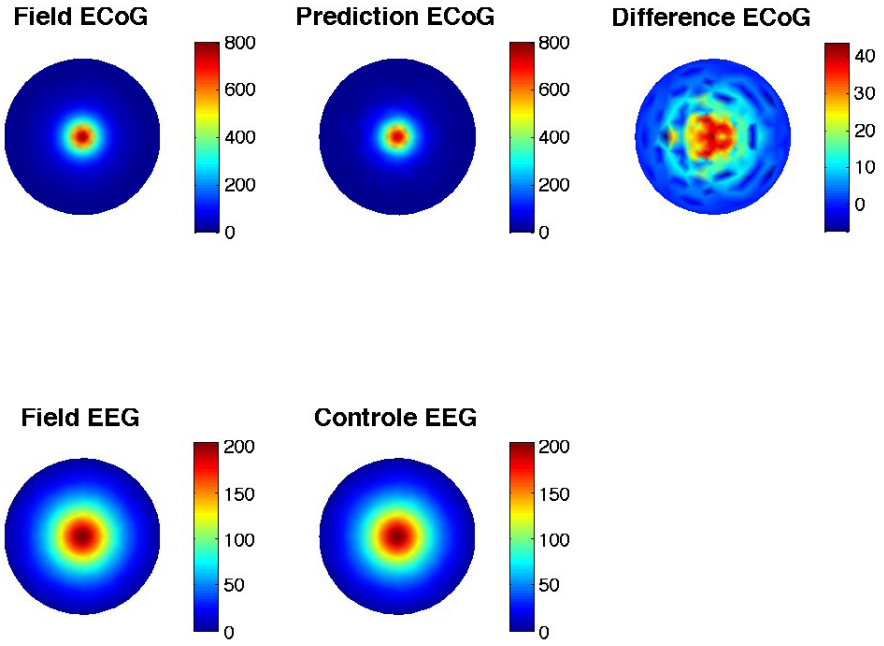

Figure 25 Predicted ECoG from simulated EEG data (upper middle, in a.u.) compared to true ECoG from dipole at (0,0,0.060) (upper left, in a.u.) and the difference between these two potentials (upper right, in a.u.). Predicted control EEG from predicted ECoG (lower middle, in a.u.) compared to true EEG (lower left, in a.u).

These small differences show that the regularization parameters are chosen correctly.

3.7 Forward problem – Predicted EEG from real data ECoG

In this section we will test the forward method on real data, measured from an epileptic patient at the University of Freiburg. We do this by calculating EEG from event related ECoG data (see Method section), via a transfer matrix.

Figure 26 shows a side view of a sphere representing the head, with the ECoG (grey circles) and EEG (red circles) electrodes projected on this sphere to illustrate their relative position. Notice that these electrodes are in fact located one two different spheres. Electrode T7 is lying directly above the ECoG grid. Electrode P7 is located near the grid, posterior to T7. We compare the results of the forward at these two locations. Like is shown from theoretical results, we expect the electrode overlying the grid to be predicted more accurate than the electrode posterior to it.

The data we used to test the forward model is an event related potential (ERP) from 100 ms before a presented accented tone (see Methods) until 500 ms after this tone. The right panel of figure 27 shows this ERP. The left panel of figure 27 shows the corresponding potential distribution over the ECoG grid at the minimum of this ERP (black asterisk, 116 ms). The measured EEG potentials at the same time are given in the left panel of figure 28. This is a top view of the left half of the head with the potentials colour coded as given in the colour bar at the right. When the ECoG potentials are used in the forward method, this results in the predicted values given in the right panel of figure 28. The relative difference between the measured EEG potentials and the predicted EEG potentials is 60% at electrode T7 and 120% at electrode P7.

If ECoG potentials of a random set of 30 times are used in the forward method, the relative differences at electrode T7 are between 15% and 84%, with a mean of 63%. The relative differences at electrode P7 are between 62% and 200% with a mean of 130%. Predicted potentials at electrode P7 are always worse than predicted potentials at electrode T7.

Figure 29 shows an example. The measured EEG potentials at time 96 ms are given in the left figure. The predicted values from the corresponding measured ECoG data are given in the right figure. The relative difference between these potentials at electrode T7 are 15% and at electrode P7 82%. Again, electrode P7 is predicted worse than electrode T7.

Although the potentials at the electrode overlying the grid are always predicted more accurate than the electrode posterior to the grid, the predicted potentials are not accurate enough. The relative differences are large, with a mean of 63%. Reasons for this are given in the discussion.

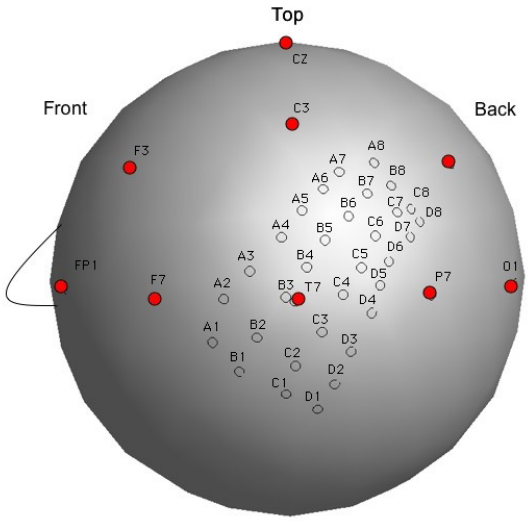

Figure 26 A side view of a head to illustrate the relative locations of ECoG electrodes (grey circles) and EEG electrodes (red circles) shown on one sphere.

4. Discussion

4.1 Differences ECoG and EEG

Simulations of EEG and ECoG show two important differences. EEG has a smaller amplitude and is broader in time with smaller high-frequency components than the ECoG signals. This has two reasons. The distance from the EEG electrode to the dipole is larger than the distance between the ECoG electrode and the dipole. The second reason, that has the largest influence, is the large resistance of the skull, which attenuates the signal amplitude.

4.2 Forward method – Simulated data

Results in this manuscript show that the forward method has relative differences between 6.6 and 11 %,for ECoG potentials known at all vertices of the inner sphere. This has two reasons. First the calculated ECoG is not accurate. Analytically the potentials can only be computed at the outermost

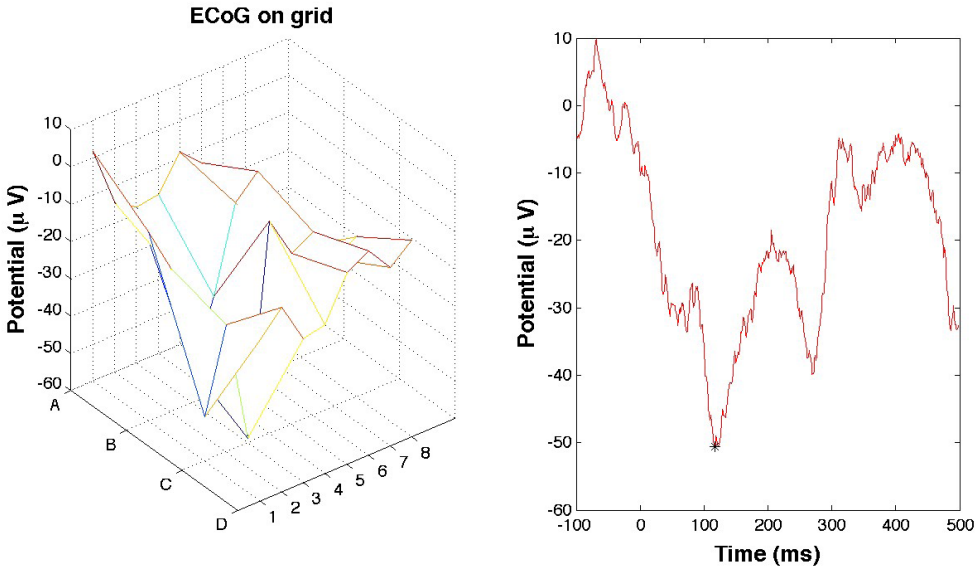

Figure 27 The right figure gives the time course of the event related potentials from the grid electrode B3. At time 116 ms (given by the black asterisk) the potential distribution over the grid is shown in the left figure, with on the x,y-plane the grid electrodes A1 to D8 and on the z-axis the potential at that specific electrode.

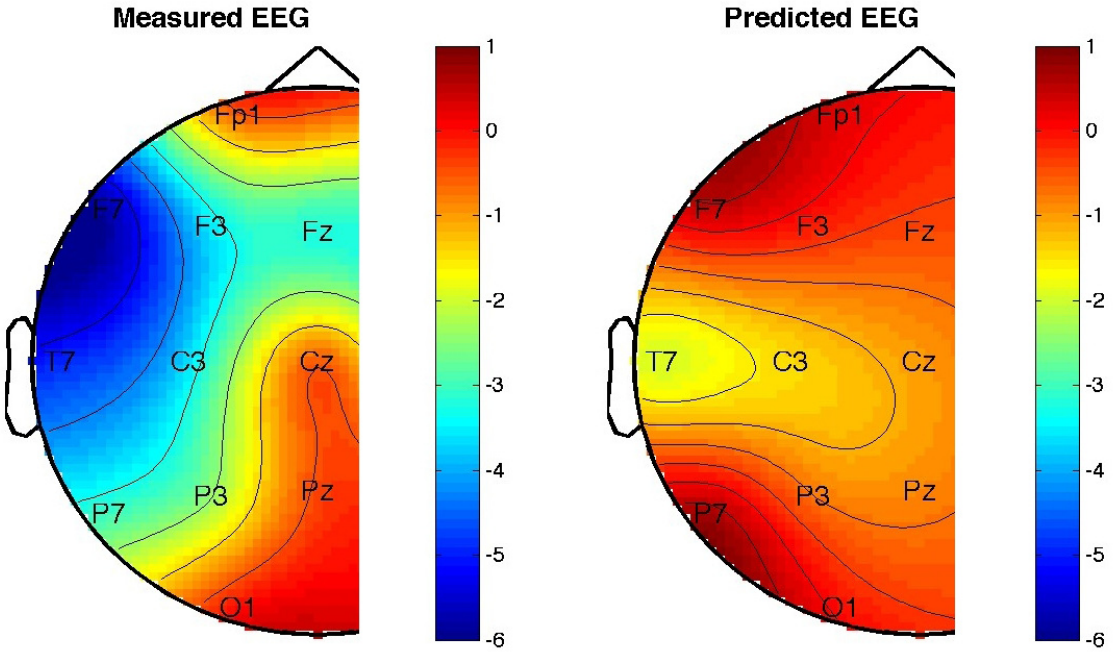

Figure 28 The EEG potentials (in □V) measured at time 116 ms (left panel) and the predicted potentials (in □V) from the corresponding ECoG (right panel). The relative difference between the potential at electrode T7, which is positioned right over the grid (see figure 28) is 60%. This is lower than the relative difference of 1.2 102 % from electrode P7, which is situated near the grid, posterior of the grid.

surface. The ECoG can only be approached by ignoring the skull and the scalp. This results in an overestimation of the ECoG potentials, which results in the end in an overestimation of the predicted EEG potentials.

Another reason for the relative difference is the numerical implementation. The discretization of the surfaces causes discrepancies between the potentials calculated analytically and with numerical methods. These discrepancies are generally between 1 and 5% and are larger for more complex and non-symmetrical geometries. Dipoles further from the centre of the spheres have more complex triangulated spheres, which results in larger errors

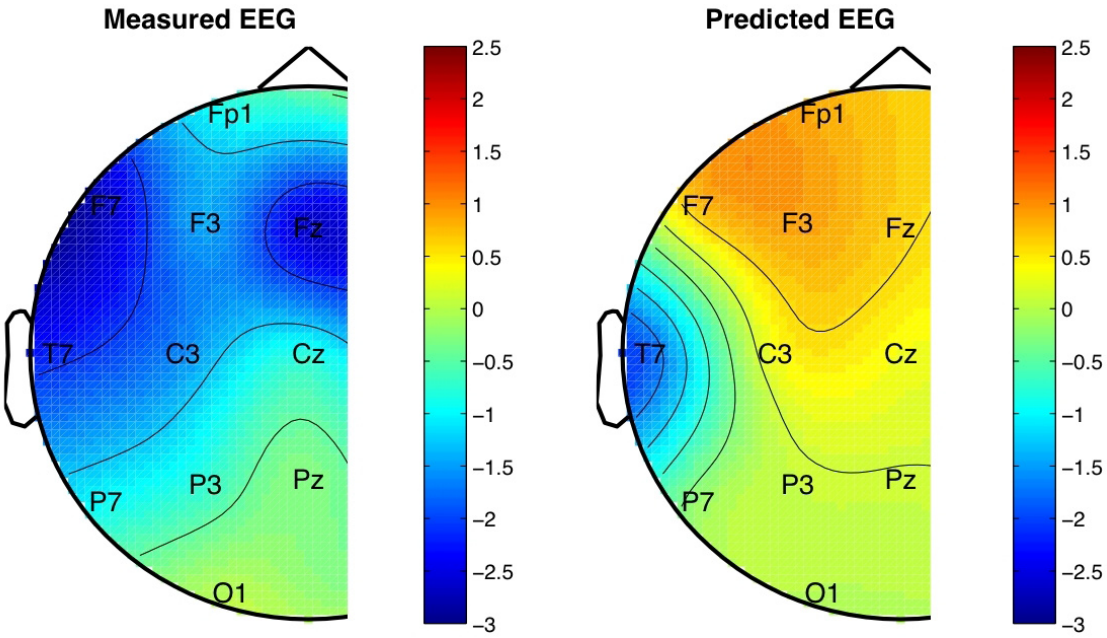

Figure 29 The EEG potentials (in □V) measured at time 96 ms (left panel) and the predicted potentials (in □V) from the corresponding ECoG (right panel). The relative difference between the potential at electrode T7, which is positioned right over the grid (see figure 28) is 15%. This is lower than the relative difference of 82% from electrode P7, which is situated near the grid, posterior of the grid.

in the predicted EEG potentials (e.g. 11% for a dipole at (0,0,0.060) compared to 7.5% for a dipole at (0,0,0)).

To solve the numerical discrepancies a refined triangulated grid can be taken. This results in more triangles projected on the spheres. A disadvantage of taking a refined grid is the loss of computational power, since there are more points at which the potential has to be computed and the transfer matrix becomes larger.

Further the results show that the forward method is more accurate for points close to the source, compared to potentials calculated at points far away from the source.

4.3 Forward method – ECoG grid and EEG grid

In reality potentials are measured with electrodes placed at some locations of the brain and at some locations of the scalp. This setup is simulated by an ECoG grid placed on the inner sphere and an EEG grid on the outer sphere. Results show that the forward method is more accurate at electrodes close to the source, for a higher resolution ECoG grid and for surface dipoles. This last finding is of practical importance, since most cognitive interesting sources for BCI applications are located in the cortex and the cortex is the outermost layer of the brain.

The forward model constructed in this manuscript needs potentials on all vertices of the inner surface. If the potentials are only simulated or measured at certain electrodes on the inner sphere, the potentials at the rest of the vertices have to be interpolated. In this manuscript we interpolated by putting constraints on the Laplacian of the potential surface (see Methods). This method assumes a smooth interpolation between successive points and maxima at points with known potentials. Using the Laplacian is not the best method, since it cannot describe the rapid potential changes in space of surface dipoles. Further it causes too slow a decay in potential to zero from the edge of the grid to the backside of the sphere. This results in an overestimation of the potentials outside the grid. For surface dipoles this causes an overestimation of the potentials at the edge of an EEG grid, whereas for deeper sources the potential of the reference EEG electrode is overestimated, which causes all potentials to drop with rereferencing. This results in an underestimation of the EEG grid potentials.

4.4 Inverse method – Simulated data

The results in this manuscript show that the inverse method has relative differences between 4.1 and 7.7%. This is due to the overestimation of the analytically produced ECoG and the numerical implementations, like in the forward method.

The fact that these relative differences are smaller than the ones from the forward method can be explained by the fact that the spheres consist of different triangulated grids. Different triangulations result in different numerical errors.

4.5 Forward method – Real data

EEG electrodes are distributed all over the head. They reflect brain activity generated all over the brain. Whereas the ECoG grid situated at the left side of the brain, reflects only the activity in the neighbourhood of the grid. With these ECoG potentials only the EEG potentials above of the grid can be predicted. We expected the potentials at the electrode overlying the grid (T7) to be estimated more accurately than the electrode posterior to the grid (P7). Relative differences are indeed between 15% and 84%, with a mean of 63% for electrode T7 and between 62% and 200% with a mean of 130% for electrode P7.

Unfortunately errors are large. A reason for this is that to place the electrodes onto the brain of our subject, the skull was opened. When the electrodes were placed and the skull and scalp were closed, there were still gaps in the skull, which cause the conductivity of the skull to be larger than implemented here and anisotropic throughout the skull. These distortions cannot be modelled in the transfer matrix, since we don't know these distortions exactly.

Another reason is the fact that we have referenced to electrode O1. This electrode is the best in our setup. It is located far from the auditory source, but still reflecting some brain activity. More convenient would be to measure and reference to an electrode on the mastoid bone, which reflects less brain activity.

A third reason is the fact that we modelled the head by three concentric spheres. It would be more convenient to implement realistic geometries for brain, skull and scalp in the forward model. These geometries can be extracted from an MRI scan of the subject's head. This will change the transfer matrix, which can result in more accurate potentials.

To reduce the brain activity unrelated to the stimulus, we took the event related potential (ERP) of the measured signals and used potentials at several times to calculate the corresponding potential distribution of the EEG at the same times. A disadvantage of averaging data is that you need more than one trial. Implementation in BCI will slow down the algorithm.

4.6 Inverse method with real data

In this manuscript we did not investigate the inverse model with measured data. The electrode placement was unsuitable for this problem. The EEG electrodes were distributed all over the head, whereas the ECoG electrode grid was very small and located at the left side of the brain, with only one EEG electrode overlying the grid and three electrodes in the neighbourhood. To get good inverse results a denser EEG electrode placement should be used, especially at locations over the ECoG grid.

5. Conclusion

We think that the forward method will work better on measured data, when some changes, like implementing realistic geometries of the head, are implemented. Especially since theoretical results show that the method is more accurate for surface dipoles than for deeper sources. Cognitive interesting sources stem from the outermost layer of the brain.

Further research is needed to see whether the inverse method can be implemented in BCI.

References

Barr, R. C., Ramsey, M., & Spach, M. S. (1977). Relating epicardial to body-surface potential distributions by means of transfer-coefficients based on geometry measurements. *Ieee Transactions on Biomedical Engineering, 24*(1), 1-11.

Birbaumer, N., Ghanayim, N., Hinterberger, T., Iversen, I., Kotchoubey, B., Kubler, A., et al. (1999). A spelling device for the paralysed. *Nature, 398*(6725), 297-298.

Farwell, L. A., & Donchin, E. (1988). Talking off the top of your head: Toward a mental prosthesis utilizing event-related brain potentials. *Electroencephalogr Clin Neurophysiol, 70*(6), 510-523.

Gulrajani, R. M. (1998). *Bioelectricity and biomagnetism*. New York; Chichester England: J. Wiley.

Hochberg, L. R., Serruya, M. D., Friehs, G. M., Mukand, J. A., Saleh, M., Caplan, A. H., et al. (2006). Neuronal ensemble control of prosthetic devices by a human with tetraplegia. *Nature, 442*(7099), 164-171.

Kavanagh, R. N., Darcey, T. M., Lehmann, D., & Fender, D. H. (1978). Evaluation of methods for 3-dimensional localization of electrical sources in human-brain. *Ieee Transactions on Biomedical Engineering, 25*(5), 421-429.

Leuthardt, E. C., Schalk, G., Wolpaw, J. R., Ojemann, J. G., & Moran, D. W. (2004). A brain-computer interface

using electrocorticographic signals in humans. *J Neural Eng, 1*(2), 63-71.

Mehring, C., Rickert, J., Vaadia, E., de Oliveira, S. C., Aertsen, A., & Rotter, S. (2003). Inference of hand movements from local field potentials in monkey motor cortex. *Nature Neuroscience, 6*(12), 1253-1254.

Oostendorp, T. F., Delbeke, J., & Stegeman, D. F. (2000). The conductivity of the human skull: Results of in vivo and in vitro measurements. *IEEE Trans Biomed Eng, 47*(11), 1487-1492.

Oostendorp, T. F., Vanoosterom, a., & Huiskamp, G. (1989). Interpolation on a triangulated 3d surface. *Journal of Computational Physics, 80*(2), 331-343.

Ramanathan, C., Ghanem, R. N., Jia, P., Ryu, K., & Rudy, Y. (2004). Noninvasive electrocardiographic imaging for cardiac electrophysiology and arrhythmia. *Nature Medicine, 10*(4), 422-428.

Wolpaw, J. R., Birbaumer, N., McFarland, D. J., Pfurtscheller, G., & Vaughan, T. M. (2002). Brain-computer interfaces for communication and control. *Clinical Neurophysiology, 113*(6), 767-791.

Wolpaw, J. R., McFarland, D. J., Neat, G. W., & Forneris, C. A. (1991). An eeg-based brain-computer interface for cursor control. *Electroencephalogr Clin Neurophysiol, 78*(3), 252-259.